Plant stiffness and biomass as drivers for drag forces under extreme wave loading: a flume study on mimics

Maike Paul[a,1,2], Franziska Rupprecht[b], Iris Möller[c], Tjeerd J Bouma[d], Tom Spencer[c], Matthias Kudella[a], Guido Wolters[e], Bregje K van Wesenbeeck[e], Kai Jensen[b], Martin Miranda-Lange[a], Stefan Schimmels[a]

[a] Forschungszentrum Küste (FZK), Merkurstr. 11, 30419 Hannover, Germany

[b] Applied Plant Ecology, Biocenter Klein Flottbek, University of Hamburg, Ohnhorststr. 18, 22609 Hamburg, Germany

[c] Cambridge Coastal Research Unit, Department of Geography, University of Cambridge, Downing Place, Cambridge CB2 3EN, UK

[d] Yerseke Spatial Ecology, Netherlands Institute for Sea Research (NIOZ), Korringaweg 7, 4401 NT, Yerseke, the Netherlands

[e] Deltares, Boussinesqweg 1, 2629 HV Delft, the Netherlands

[1] Present address: Institute of Geoecology, Technische Universität Braunschweig, Langer Kamp 19c, 38106 Braunschweig, Germany

[2] corresponding author, m.paul@tu-braunschweig.de

Abstract

Moving water exerts drag forces on vegetation. The susceptibility of vegetation to bending and breakage determines its flow resistance, and chances of survival, under hydrodynamic loading. To evaluate the role of individual vegetation parameters in this water-vegetation interaction, we conducted drag force measurements under a wide range of wave loadings in a large wave flume. Artificial vegetation elements were used to manipulate stiffness, frontal area in still water and material volume as a proxy for biomass. The aim was to compare: (i) identical volume but different still frontal

area, (ii) identical stiffness but different still frontal area, and (iii) identical still frontal area but different volume.

Comparison of mimic arrangements showed that stiffness and the dynamic frontal area (i.e., frontal area resulting from bending which depends on stiffness and hydrodynamic forcing) determines drag forces. Only at low orbital-flow velocities did the still frontal area dominate the force-velocity relationship and it is hypothesised that no mimic bending took place under these conditions.

Mimic arrangements with identical stiffness but different overall material volume and still frontal area showed that forces do not increase linearly with increasing material volume and it is proposed that short distances between mimics cause their interaction and result in additional drag forces. A model, based on effective leaf length and characteristic plant width developed for unidirectional flow, performed well for the force time series under both regular and irregular waves. However, its uncertainty increased with increasing interaction of neighbouring mimics.

Key words

drag force, wave forcing, plant mimics, stiffness, biomass, frontal area

1. Introduction

It has been widely recognised that the interaction of flexible littoral vegetation (e.g. seagrass, salt marsh) with both oscillatory and unidirectional flow in shallow marine environments leads to a reduction of water velocity and hydrodynamic energy (Lightbody and Nepf, 2006; Möller et al., 1999; Yang et al., 2012). Moreover, recently Möller et al. (2014) showed that a transplanted salt marsh is even capable of substantial wave height reduction under simulated storm surge conditions. Given the increasing need for coastal protection, there is high interest in nature-based coastal defence. Using intertidal vegetation in such schemes is one of the most promising approaches to date (Barbier et al., 2008; Bouma et al., 2014; Temmerman et al., 2013). However, implementing such nature-based coastal defence schemes requires high quality modelling capability of flow and wave dissipation by

vegetation fields, and hence a mechanistic understanding of vegetation-hydrodynamic interaction. The flow reducing capacity of vegetation is based on the drag the vegetation exerts on the flow (either unidirectional or oscillatory) which can be expressed by the drag coefficient C_D. In return, the vegetation canopy is exposed to these drag forces and its resistance to these determines its survival (Callaghan et al., 2007; Denny et al., 1998). Estimation of these forces has therefore received considerable attention from both the hydraulic (Chen et al., 2011; Henry and Myrhaug, 2013; Siniscalchi et al., 2012) and ecological (Carrington, 1990; Gaylord et al., 2003; Sand-Jensen, 2003) research communities.

The drag expressed by C_D can be used to estimate the rate of frictional dissipation which leads to the reduction of wave energy (Dalrymple et al., 1984). Several models have been developed to estimate C_D from wave and vegetation parameters (Dalrymple et al., 1984; Kobayashi et al., 1993; Maza et al., 2013; Méndez and Losada, 2004), expressed as a function of either the Reynolds number *Re* or the Keulegan-Carpenter number *KC* (see Henry et al. (2015) for a comprehensive review). These models have been applied to wave dissipation datasets from both field (Bradley and Houser, 2009; Paul and Amos, 2011) and laboratory studies (Augustin et al., 2009; Houser et al., 2015; Stratigaki et al., 2011) in low to medium energy wave conditions. Dissipation of waves with heights in excess of 20 cm in water depths greater than 1 m above a typical salt marsh canopy has so far only been measured by Möller et al. (2014) in a large wave flume, and by Yang et al. (2012) in the field. Möller et al. (2014) show that under high incident wave energy levels the structural integrity of the vegetation elements is exceeded and plant elements begin to fold and break, rather than flex and bend as they do in response to low to medium energy conditions. As vegetation response changes with changing hydrodynamic forcing, a drag coefficient which assumes plant rigidity can thus not necessarily be used to calculate the drag forces acting on the vegetation, particularly when extrapolating to extreme conditions (Bell, 1999). It is thus necessary to determine the drag forces acting on salt marsh vegetation directly, in order to assess its susceptibility to physical damage during storm surges. Only then will it be possible to properly assess vegetation resilience under such conditions.

Available direct measurements of drag forces on natural plants are scarce and, due to the restricted dimensions of most flumes, typically limited to small waves (wave height $H \leq 7$ cm) or low-velocity unidirectional flow (Bouma et al., 2005; Bouma et al., 2010). Laboratory measurements with two intertidal plant species (*Spartina anglica* and *Zostera noltii*) showed that under those relatively benign conditions, the drag forces decrease with decreasing stiffness and suggest that bending of the flexible plants causes this reduction (Bouma et al., 2005). This observation agrees well with other research undertaken on drag reduction and reconfiguration (Boller and Carrington, 2006; O'Hare et al., 2007; Siniscalchi and Nikora, 2012), indicating that the effective frontal area after reconfiguration is a major factor in explaining drag. On the other hand, systematic studies with both real (Bouma et al., 2010; Paul and Amos, 2011) and artificial (Paul et al., 2012) flexible coastal vegetation suggests that wave attenuation, and hence C_D, in shallow water environments is governed by the amount of above ground standing biomass rather than by individual parameters such as leaf length or vegetation stiffness. This observation is also supported by a study on fresh water macrophytes (Penning et al., 2009).

According to theory, the drag force *F* acting on a plant, is related to the frontal surface area *A* which in return depends on vegetation stiffness (Aberle and Järvelä, 2013; Bouma et al., 2010). This relationship can be described as

$$F = \frac{1}{2}\rho C_D A u^{\beta} \qquad (1)$$

where ρ is density of water, *u* is water velocity and β is a tuning parameter which depends on the streamlining of the plant, typically <2 for flexible objects, and 2 for rigid objects (Vogel, 1994). Biomass is not explicitly included in this equation but biomass investments in stem material will typically be reflected in shoot stiffness and thus plant shape (Bouma et al., 2010). To account for reconfiguration in equation 1, the parameters C_D, *A,* β or a combination of these three have been used. Statzner et al. (2006) for instance propose to change C_D and/or *A* to account for plant reconfiguration, while Denny and Gaylord (2002) suggest the maximum projected area to be a constant *A* and to reflect shape changes in C_D and β. Luhar and Nepf (2011) have argued that plant posture, i.e. the flow-dependent

104 position of the plant and all its components within the water, affects streamlining and frontal area and
105 express this change through an 'effective leaf length'. They thus advocate constant C_D and β and
106 propose *A* to be the product of a constant characteristic width and a variable effective leaf length. In
107 addition to having only one variable parameter, the latter model has the advantage that all necessary
108 parameters can be derived from material properties and flow measurements and do not require
109 knowledge of plant posture. However, the model has so far only been validated under unidirectional
110 flow.

111 From the existing data, it appears that vegetation stiffness (and resulting frontal area for any
112 given applied force) and biomass are both key drivers in wave attenuation and associated drag forces.
113 However, their respective relative importance in determining drag force and their potential
114 interactions are not yet well understood. In order to unravel these relationships and improve the
115 assessment of drag forces based on vegetation parameters, we conducted controlled experiments with
116 plant mimics - in the form of flexible plastic strips - under a range of wave conditions. These strips were
117 combined in such a way, that we maintained either (i) a constant frontal area, but with varying biomass
118 (i.e., same number of strips but with different thickness; 8 x 1 mm strips vs. 8 x 2 mm strips), (ii) an
119 identical biomass, but a contrasting frontal area (i.e., few thick strips or more thin strips to obtain a
120 constant volume; 8 x 1 mm strips, 4 x 2 mm strips or 2 x 4 mm strips) or (iii) an identical stiffness
121 between shoots, but a contrasting frontal area (i.e., contrasting numbers of identical strips; 4 x 2 mm
122 strips vs. 8 x 2 mm strips). Moreover, we used the obtained data to evaluate whether or not the model
123 based on effective leaf length (Luhar and Nepf, 2011) is also applicable to drag forces under the
124 oscillatory motion of waves. Whilst we appreciate that coastal vegetation is often exposed to breaking
125 waves in the swash zone, we limited our tests to non-breaking waves. This approach reduces the
126 complexity of hydrodynamics, allowing us to focus on the effect of frontal area, biomass and stiffness
127 of the vegetation elements. For the first time, the direct drag measurements in this study also covered
128 wave loading under extreme events. The measurements reported here will, in particular, help improve

129 existing drag models and, in general, inform future studies on vegetation resilience to high energy
130 wave forcing.
131
132 **2. Methods**
133 Experiments were carried out in conjunction with tests of wave attenuation over natural salt marsh
134 transplants (Möller et al., 2014). They were conducted in the 5 m wide, 7 m deep and approx. 310 m
135 long Large Wave Flume (GWK) of the Forschungszentrum Küste (FZK) in Hannover, Germany.
136
137 2.1. Model setup
138 An elevated test section of 60 m length was constructed approx. 95 m from the wave paddle which
139 raised the salt marsh and drag sensors 1.5 m above the flume floor. This was necessary to ensure
140 sufficient water depth at the wave paddle to generate the desired waves and to allow waves to fully
141 develop before reaching the test section. At the beginning of the test section, a concrete ramp with a
142 slope of 1:1.7 for 1.2 m, followed by a slope of 1:10 over a distance of 7 m, was installed to allow for a
143 smooth transition of waves (Figure 1a). Here waves shoaled, but did not break, before interacting with
144 the strip arrangements for all treatments considered here. At the end of the test section, a gravel slope
145 (1:10) was constructed for the same purpose. Wave breaking at the 1:6 asphalt slope at the end of the
146 flume minimised wave reflection and active wave absorption of the wave maker was employed for the
147 same purpose.
148 On the level test platform, 7.15 m away from the front edge, five drag sensors were deployed in a line
149 normal to the direction of wave approach with the sensor heads flush with the flume floor. The drag
150 sensors were installed 30 cm apart starting 106 cm from the flume wall (Figure 1b). They operated on
151 the principle of a wheatstone bridge (Carrington, 1990; Denny, 1988) and measured forces in two
152 directions up to 10 N (accuracy ±0.5% F.S., developed by Deltares). They were deployed to capture
153 forces in the direction of, and counter to, wave propagation along the flume. An electromagnetic
154 current meter (EMCM) was also deployed on the same cross-section, located 76 cm from the flume

wall (Figure 1b). The EMCM was set to record point measurements at a height of 15 cm above the test platform. This height corresponds to half the height of mimic arrangements which were slightly set off the ground by the metal bar fitting (Figure 1c). It was chosen as a representative value for the bulk velocity acting on the arrangements for the non-uniform velocity profile under wave motion. Data from all instruments was collected simultaneously at a sampling rate of 100 Hz.

A range of wave conditions (wave heights of between 0.1 and 0.9 m and wave periods between 1.4 and 5.1 s) was applied in two different water depths (1 and 2 m above the test platform), using both regular and irregular waves. Irregular waves were generated with a JONSWAP spectrum (peak enhancement factor 3.3) over 1000 waves and then followed by a regular wave test run (n = 100 waves) with a wave height corresponding to the zeroth-moment wave height (H_{m0}) of the irregular test. Active wave absorption at the end of each test and sufficient waiting time ensured that all tests started with still water level. Not all tests yielded drag data, due to overloading of the sensors or instrument failure; these tests were excluded from the subsequent analysis.

2.2. Plant mimics

For the force measurements in the flume, plastic strips attached to the drag sensors were used as a simplified representation of vegetation, or vegetation mimic, with varying degrees of stiffness. While the strips do not represent a particular plant species, they enabled us to easily manipulate individual parameters and hence assess their effect on drag in a more controlled fashion than would have been possible with real plants. A horizontal metal bar was mounted on each drag sensor and oriented normal to the wave direction. On the metal bars of four drag sensors different sets of plastic strips were mounted (Figure 1c). The fifth drag sensor was fitted with the horizontal metal bar but without any of the plastic strips to allow recording of the drag forces exerted on the mounting-bar alone as an experimental control treatment. Strips were all cut from Lexaan plates (mass density 1240 kg m^{-3}) to a standard length and width of 25 cm and 0.55 cm respectively, but using plates of three different thicknesses (1, 2, and 4 mm). Lexaan was selected as it is a highly flexible type of plastic but shows a

distinct difference in stiffness between the three material thicknesses chosen here. Thicknesses were chosen so as to ensure that all mimics had sufficient rigidity to make their movement stiffness-dominated rather than buoyancy-dominated (Luhar and Nepf, 2011) and were yet flexible enough to be considered non-rigid. By varying the material thickness (simulated 'stiffness') the bending behaviour and hence frontal area was varied while keeping the material properties identical for ease of comparison.

In addition, the number of strips per drag sensor was varied to achieve a range of different material volumes (simulated 'biomass') per drag sensor exposed to the same experimental conditions (Table 1). To characterise the material, its flexural rigidity was derived by a 3-point-bending test according to the methodology described by Rupprecht et al. (2015). A sample was placed horizontally across two supporting bars spaced 15 times the sample thickness and the centre was pushed down with a third bar. The force required to push the sample down a given distance was recorded and the slope of the force-distance relationship (P/h) was used to determine flexural rigidity (*J*):

$$J = \frac{\left(\frac{s}{2}\right)^3 P}{6h} \qquad (2)$$

where *s* is the distance between supporting bars (Paul et al., 2014).

2.3. Data processing

Horizontal orbital velocities were obtained from the EMCM time series. To eliminate noise from the signal, a Fast Fourier Transformation was conducted on the whole time series and a low pass filter (f_l = 0.7 Hz) applied. For regular wave tests, the data were re-transformed into the time domain and the first 11 fully developed waves were used for subsequent analysis (Figure 2a). This eliminated any effects caused by reflection from the end of the flume. Zero-upcrossing was used to identify individual waves from the horizontal component of the velocity data and determine maximum horizontal orbital velocity $u_{r,max}$ and period T_r for each wave. This data was then averaged to yield a single value for each test. Moreover, time series of the individual waves were averaged to obtain a representative wave velocity time series at 15 cm above the test platform. To reduce noise in the representative time series, the longest and shortest wave in each record were removed, resulting in n = 9 for averaging.

For the irregular wave tests, elimination of reflection and averaging were not possible and consequently the whole time series of fully developed waves was used for spectral analysis using Fast Fourier Transformation. An additional high pass filter (f_p/2.1, f_p = peak frequency) was applied and a representative horizontal orbital velocity ($u_{i,m0}$) (analogue to standard wave height analysis) computed

$$u_{i,m0} = 4\sqrt{\sum_{j=1}^{m} \mathrm{S(f)}_j \Delta \mathrm{f}} \qquad (3)$$

where m is the total number of frequency components, $S(f)$ is the velocity spectrum and Δf the frequency band width. Values refer to the measurement point 15 cm above the bed which corresponds to half the mimic arrangement height and is considered the location where the flow is representative of the bulk velocity acting on the mimics. Processing of time series for drag forces was done analogous to horizontal orbital velocities to obtain F_r for regular and F_{m0} for irregular wave tests. F_{m0} is the force derived from the 0th moment of the force spectrum $S_F(f)$ and hence a representative parameter to describe the force acting by the waves constituting the applied wave spectrum.

To remove the impact of the horizontal bar to which the mimics were attached (Figure 1c), control runs with the strip-free bar were processed first. Consecutively, a best fit for $F_{control} \sim u^2$ in correspondence with the Luhar and Nepf (2011) model was found for regular and irregular waves, respectively:

$$\mathrm{F_{r,control}} = 0.53\mathrm{u}|\mathrm{u}| \qquad (4)$$

$$\mathrm{F_{m0,control}} = 0.22\mathrm{u}|\mathrm{u}| \qquad (5)$$

From these relationships, control time series were computed for each test run and subtracted from the raw force time series for each mimic arrangement prior to processing according to the above protocol.

2.4. Modelling

To estimate mimic posture without knowledge of its bending angle, the buoyancy parameter *B* and the Cauchy number *Ca*, i.e. the two dimensionless parameters driving plant posture, were derived (Luhar and Nepf, 2011).

$$B = \frac{\Delta\rho g b t l^3}{J} \quad (6)$$

$$Ca = \frac{1}{2}\frac{\rho C_D b u^2 l^3}{J} \quad (7)$$

where Δρ is the difference in density between water and the mimic. As mentioned above, plant posture affects streamlining and thus frontal area. The latter can be expressed by the effective leaf length l_{eff} (Luhar and Nepf, 2011):

$$l_{eff} = \left(1 - \frac{(1-0.9Ca^{-1/3})}{1+Ca^{-3/2}(8+B^{3/2})}\right) l \quad (8)$$

Substituting into eq. 1 and using β = 2 as proposed by Luhar and Nepf (2011) allows estimation of the drag forces for regular and irregular waves respectively, from velocity measurements:

$$F_{modelled} = \frac{1}{2}\rho C_D b l_{eff} u^2 \quad (9)$$

with C_D = 1.95 for a rigid, upright blade (Vogel, 1994). To capture negative forces under the wave trough, u^2 was replaced by $u|u|$ in eq. 9. The model was applied to the averaged time series for regular waves based on the first 11 fully developed waves in the record and the full time series for irregular waves by substituting *u* in eq. 9 with $u_{r,max}$ and $u_{i,m0}$ obtained from the time series recorded 15 cm above the bed, respectively. This modelled time series was then processed analogous to the measured force time series to obtain $F_{r,model}$ and $F_{m0,model}$ respectively. The goodness-of-fit for the Luhar and Nepf (2011) model was assessed using linear regression in the averaged time series for regular, and the full time series for irregular, waves. All data pre-processing was done in L~davis (provided by FZK) and processing as well as statistical analysis was conducted in MATLAB®.

3. Results

Throughout all experimental conditions, the force recorded by the drag sensors with metal bars but without plastic strips was generally low (F_r < 0.4 N and F_{m0} < 0.5 N). However, at low velocities the strip

255 mounting bars accounted for up to 19% of the measured forces for any strip arrangement at a given
256 horizontal orbital velocity. The metal bar's influence was therefore removed from the force
257 measurements during pre-processing.
258
259 3.1. Measured drag forces
260 Time series of forces and horizontal orbital velocities during regular and irregular wave tests showed
261 that the forces changed direction in correspondence with the wave orbital cycle. However, forces were
262 not necessarily in phase with the hydrodynamic loading (Figure 2b-e). No systematic response could
263 be detected, with forces leading velocity in some cases (e.g. Figure 2b) and lagging velocity in others
264 (e.g. Figure 2e). The phase lag may result from different bending behaviour of the mimics depending
265 on their stiffness and the wave period. However, no video footage of the mimics was available to
266 explore the link of these phase differences to mimic motion in detail.
267 For all strip arrangements, the acting forces increased with increasing horizontal orbital velocity, both
268 for regular (Figure 3a) and irregular waves (Figure 3b). In both cases, the strip arrangement with the
269 highest volume (8 x 2 mm) yielded forces that were on average 1.9 and 2.7 times higher than forces
270 for the arrangements with half the volume (8 x 1 mm and 4 x 2 mm, respectively).
271 At low orbital velocities under regular waves ($u_{r,max}$ < 0.4 m s^{-1}), frontal area appeared to influence drag
272 forces, as the three arrangements with identical volume but different number of strips per
273 arrangement (i.e. 8 x 1 mm, 4 x 2 mm and 2 x 4 mm) resulted in forces increasing with increasing
274 number of strips per arrangement (Figure 3a). The forces recorded with the 8 x 1 mm and 4 x 2 mm
275 arrangements exceeded those recorded with the 2 x 4 mm arrangement by a factor of 1.2 and 2.3
276 respectively. With increasing $u_{r,max}$ the difference between the 8 x 1 mm and 4 x 2 mm strip
277 arrangement reduced and recorded forces became comparable in the velocity range 0.4 - 0.7 m s^{-1}
278 when the standard deviations are considered. Beyond $u_{r,max}$ = 0.7 m s^{-1}, forces on the 4 x 2 mm
279 arrangement exceeded those for the 8 x 1 mm arrangement, while values for the 2 x 4 mm
280 arrangement increased more rapidly with increasing velocities but still remained lower than for the

other arrangements across the whole velocity range tested. Comparing the 4 x 2 mm and 8 x 2 mm arrangement for regular waves shows that material volume has an effect on drag forces, but that this effect is neither linear nor constant. At low velocities the 8 x 2 mm arrangement yielded more than three times the forces measured for the 4 x 2 mm arrangement (3.17 for $u_{r,max}$ = 0.2 m s^{-1}), while this difference decreased to a factor of 2.10 for $u_{r,max}$ = 0.59 m s^{-1}.

The influence of frontal area on drag forces at low velocities was also visible for irregular waves ($u_{i,m0}$ < 0.8 m s^{-1}). Similar to regular waves, the difference in forces measured with the 8 x 1 mm and 4 x 2 mm arrangement reduced with increasing $u_{i,m0}$ until they merged onto approx. one line for $u_{i,m0}$ > 1 m s^{-1} (Figure 3b). In contrast to the regular wave tests, however, forces observed with the 2 x 4 mm arrangement remained consistently a factor of approx. 2 lower than for the other arrangements with identical volume. Doubling the volume at constant material stiffness (i.e. from the 4 x 2 mm to 8 x 2 mm arrangement) led to an increase of drag forces by a factor of 2.06 - 2.81. In the same way as for regular waves, this factor decreased with increasing velocity.

Across all flow velocities tested, forces under irregular waves remained below those for corresponding regular wave tests (Figure 4). This can be attributed to the different computation methods used to derive statistical values from the measured force time series; F_r refers to the maximum force in the wave cycle, while F_{m0} is a statistical parameter describing the whole spectrum which includes all waves in the spectrum.

3.2. Modelled drag forces

Flexural rigidity (Table 1) was used to estimate the effective leaf length l_{eff} in order to apply the Luhar and Nepf (2011) model to the data. The model provided a very good fit (R^2 > 0.93) for the averaged force time series for most mimic arrangements in all regular wave tests (Figure 2b-e). Even in cases with deviations in the maximum and minimum forces in the wave cycle (Figure 2e), the model captured the overall shape of the force time series and also reproduced the reduced rate of change in forces during flow reversal. Comparing modelled and measured values for F_r over the whole velocity range tested showed a very good fit (Table 1), with a slight underprediction for mimics of 1 and 2 mm

307 thickness. Forces recorded by the 2 x 4 mm arrangement were overpredicted at high velocities (Figure
308 4). The model indicated that forces for the 4 x 2 mm arrangement exceeded the ones for the 8 x 1 mm
309 arrangement for $u_{r,max}$ > 0.47 m s^{-1}. Comparison of the modelled relationships showed that mimic
310 thickness, and hence stiffness, affects forces in the low velocity ranges. The thicker, i.e. stiffer, the
311 mimic is, the higher is the velocity at which the force-velocity relationship becomes approx. linear and
312 the steeper the slope of this linear section becomes.
313 Similar to the pattern under regular waves, the model reproduced the time series of forces well for
314 irregular wave tests. Scatter plots (Figure 5) show that high forces under wave crests were generally
315 slightly underpredicted, while an overprediction of forces under wave troughs occurred in some cases
316 (e.g. Figure 5d). Considering the F_{m0} values across the whole velocity range tested, the quality of model
317 fit remained very good (Table 1, Figure 4), but showed a stronger underprediction for the 8 x 2 mm
318 arrangement than for the 4 x 2 mm arrangement. These findings suggest that stiffness was not the
319 driving parameter in this case as stiffness was identical for both arrangements. The model shows forces
320 for the 4 x 2 mm arrangement to exceed the ones for the 8 x 1 mm arrangement for $u_{i,m0}$ > 1.28 m s^{-1}
321 and, despite the model's tendency for underprediction, this agrees well with the measured data, where
322 such a ratio first occurred at $u_{i,m0}$ > 1.26 m s^{-1} (Figure 3).
323
324 **4. Discussion**
325 In this study, vegetation mimic arrangements with different volume, stiffness and still frontal area were
326 exposed to a wide range of wave forcing. Drag forces acting on the mimics were both measured directly
327 and modelled using the concept of effective leaf length. The resulting model, initially developed under
328 unidirectional flow, was applied to forces under oscillatory flow and performed well for regular as well
329 as irregular waves. In addition, comparison of measurements and model revealed that plants within a
330 patch may interact with each other in the cross-stream direction which can have strong implications
331 for vegetation stability, sediment trapping and the characterisation of vegetated foreshores.
332

333

334 4.1. The effect of frontal area on drag forces

335 Under a given hydrodynamic forcing, the flexural rigidity determines l_{eff} which, under unidirectional
336 flow, has been shown to be directly related to the drag force acting on the plant or mimic (Luhar and
337 Nepf, 2011). This study applied the concept of effective leaf length and the resulting model to forces
338 under oscillatory flow. Overall, the model performed well for time series and statistical parameters,
339 i.e. F_r and F_{m0}, under both regular and irregular waves. The slight underprediction of forces may be due
340 to the fact that the model was originally derived for unidirectional flow. The difference is likely to be
341 caused by additional inertia forces which apply due to acceleration under waves (Denny et al., 1998);
342 these forces increase with increasing horizontal orbital velocity. The data reflects this increase, as the
343 model's goodness-of-fit reduces with increasing $u_{r,max}$ and $u_{i,m0}$ (Figure 4 and 5). However, in order to
344 evaluate whether forces under waves are higher for the same flow velocity compared to unidirectional
345 flow, comparative force measurements need to be conducted in the future. An additional aspect is
346 that l_{eff} is by definition less than, or equal to, the physically deflected height as it accounts for
347 streamlining in addition to the reduced frontal area due to bending (Luhar and Nepf, 2011).
348 Streamlining may not apply to the mimics under waves and the use of the physically deflected height
349 may be more appropriate in this case. At high velocities ($u_{r,max} > 0.77$ m s^{-1}), the live *Elymus athericus*
350 plants were found to fold over at the base and streamline to a flat position for some time during the
351 wave cycle (Möller et al., 2014). The similarity between *Elymus athericus* and the mimics in terms of
352 their material properties suggest that their bending behaviour under the same hydrodynamic forcing
353 may be similar as well. Furthermore, the data for regular waves suggest that mimic response changes
354 with increasing velocities. At low ($u_{r,max} < 0.4$ m s^{-1}) velocities, mimic bending appears to be so low that
355 all mimic arrangements remain fully upright. As a consequence, still frontal area at a constant material
356 volume (i.e. mimic arrangements 8 x 1 mm, 4 x 2 mm and 2 x 4 mm) determines drag forces rather
357 than flexural rigidity (Figure 3). At intermediate velocities (0.4 m s^{-1} < $u_{r,max}$ < 0.7 m s^{-1}) different bending
358 angles of the 8 x 1 mm and 4 x 2 mm arrangement lead to similar l_{eff} and hence comparable drag forces.

359 Att $u_{r,max}$ > 0.7 m s^{-1} different bending behaviour due to different mimic stiffness between all three
360 arrangements leads to deviations in l_{eff} and hence no direct relationship between mimic properties and
361 drag forces. To assess changes in deflected height with increasing orbital velocity and to evaluate the
362 relationship of deflected height and l_{eff}, future work should include visual observations of the mimics'
363 motion and bending angle.
364
365 4.2. The effect of stiffness on drag forces
366 The similar forces for the 8 x 1 mm and 4 x 2 mm arrangement with identical material volume at high
367 velocities suggest that, in this exposure range, drag forces on vegetation depend on material volume
368 (i.e. above ground standing biomass) rather than stiffness. This finding agrees with previous
369 observations (Bouma et al., 2010; Paul and Amos, 2011; Penning et al., 2009), although it should be
370 noted that these studies only covered a limited velocity range due to practical reasons. The results
371 over the wider range of velocities presented here emphasise the fact that conclusions drawn from
372 small datasets need to be evaluated with care and that extrapolation to other velocity ranges may not
373 be possible (Bell, 1999). Considering the whole range of velocities tested here, material stiffness
374 described by flexural rigidity *J* appears to play an important role in the force-velocity relationship
375 across the whole velocity range as it determines the slope of this relationship (Figure 4). This
376 observation agrees well with data obtained under unidirectional flow (Aberle and Järvelä, 2013;
377 Callaghan et al., 2007). In regions with low wave forcing and hence low orbital velocities (i.e. a salt
378 marsh high in the tidal frame) it may therefore be beneficial for a plant to produce thicker yet stiffer
379 stems if this reduces the frontal area exposed to hydrodynamic forcing. Conversely, in regions with
380 higher wave forcing (such as a pioneer salt marsh edge), vegetation viability may benefit from the
381 presence of more flexible shoots with respect to drag forces, even if this increases the plant's frontal
382 area in still water. Such a gradient of stiffness with exposure to hydrodynamic forcing has been
383 described by Rupprecht et al. (2015). They found an increase in Young's bending modulus from the low

384 marsh species *Puccinellia maritima* (737-1995 MPa) to the high marsh species *Elymus athericus* (1952-
385 4082 MPa).
386
387 4.3. The effect of material distribution on drag forces
388 When considering mimic arrangements with identical stiffness (i.e. 4 x 2 mm and 8 x 2 mm), an effect
389 of material volume and frontal area on drag forces was observed (Figure 3). The fact that forces did
390 not exactly double between the two mimic arrangements at a given velocity can potentially be
391 attributed to the different distances between the individual model strips. The closer the strips are
392 positioned together, the more they will influence each other through the turbulence generated at their
393 edges (Sparboom et al., 2006) which is likely to lead to increased overall forces acting on the
394 arrangement. This would also explain the reduced quality in model fit between the 8 x 2 mm and 4 x 2
395 mm arrangement (Figure 4b and d) as the model was developed for individual plants, making it unable
396 to consider interactions between structures. To capture these effects of strip interaction and thus
397 account for more complex plant geometries, computation of the characteristic width *b* would need to
398 be modified. In this experiment, the model was applied by using the strip width to calculate the
399 buoyancy parameter *B* and the Cauchy number *Ca*, while the product of strip width and number of
400 strips was used in eq. 9 to compute the modelled force. This approach assumes a single solid strip and
401 does not account for the effect of complex structures with gaps between individual elements.
402 Consequently, the model in its current form predicts exactly twice the force for the 8 x 2 mm
403 arrangement than for the 4 x 2 mm arrangement. Unfortunately, the used mimic arrangements did
404 not allow for a more detailed parameterisation of the effective width. Systematic tests with defined
405 gap sizes between strips are required to close this knowledge gap in the future.
406 The dependence of drag forces on cross-stream gap size indicates that forces acting on plants when
407 positioned within a vegetation patch are more complex than previously suggested. Investigations of
408 wave forces in patches of macroalgae have shown that individual specimens can reduce the forces
409 acting on them by 'hiding' behind upstream organisms (Carrington, 1990; Eckman et al., 1994). Force

410 measurements on rigid and flexible structures under unidirectional flow have demonstrated that both
411 down-stream and cross-stream distance between structures affect acting forces (Schoneboom et al.,
412 2010; Schoneboom et al., 2011), but that both distances are related to the wake flow structure of
413 upstream elements in different array setups (offset vs. in line). The absence of upstream or
414 downstream structures in this study suggests that neighbouring vegetation stems can be assumed to
415 cause the observed patterns of enhanced drag forces when plants grow more closely spaced laterally.
416 Consequently, a threshold vegetation spacing may exist below which the shading effect of upstream
417 plants outweighs the additional forces from neighbouring stems. This threshold spacing would,
418 however, depend upon wake evolution and therefore on vegetation diameter and complexity of shape
419 as well as hydrodynamic forcing. Vegetation spacing is an important factor in marsh ecology, as marsh
420 vegetation typically needs to surpass a density threshold for significant sediment accretion to occur
421 (Bouma et al., 2009; Peralta et al., 2008). Hence we advocate further study of the effect of vegetation
422 spacing on acting forces and sediment transport to enhance our knowledge both from a hydrodynamic
423 as well as an ecological point of view.
424
425 **5. Conclusions**
426 In this study, we conducted direct force measurements on mimic arrangements representing
427 vegetation elements of varying stiffness and material volume characteristics. All mimic arrangements
428 were exposed to hydrodynamic forcing under regular and irregular waves, covering a wide range of
429 conditions including high energy events.
430 The results confirm that vegetation stiffness, rather than biomass, is the driving parameter behind the
431 force-velocity relationship as it is stiffness that determines bending and hence effective leaf length
432 under hydrodynamic forcing. Under low forcing, forces are distributed according to the still frontal
433 area of the mimic arrangement; this may be due to the lack of bending under these conditions. While
434 under increased orbital velocities, the combination of characteristic width and bending can lead to the
435 same response for mimic arrangements with identical material volume but different still frontal area.

436 Moreover, the observations of different mimic arrangements suggest that plants within a patch
437 interact with each other in the cross-stream direction. If shoots grow close enough to each other, the
438 turbulence at their edges will affect neighbouring plants and increases the drag force acting on them
439 even if the plants are not in direct contact with each other.
440 The force measurements were also modelled, applying the model based on effective leaf length by
441 Luhar and Nepf (2011) to orbital velocities. Overall, the model performed very well and was able to
442 reproduce force time series for regular as well as irregular waves. However, it did not reproduce the
443 force increase due to the interaction of neighbouring mimics which led to small deviations between
444 modelled and measured data. In order to incorporate these interactions in the model and allow for its
445 application to more complex plant shapes, visual observations alongside force measurements are now
446 required for different mimic configurations. Such work would further develop existing models, improve
447 characterisation of vegetated foreshores and aid better design of soft engineering interventions on
448 low-lying sedimentary shorelines.
449
450 **Acknowledgements**
451 We thank all of the staff at the Grosser Wellenkanal as well as B. Evans, J. Tempest, K. Milonidis and
452 C. Edwards, Cambridge University, and D. Schulze, Hamburg University, for their invaluable logistical
453 assistance. Our gratitude also goes to two anonymous reviewers whose comments greatly helped to
454 improve the manuscript. The work described in this publication was supported by the European
455 Community's 7th Framework Programme through the grant to the budget of the Integrating Activity
456 HYDRALAB IV, Contract no. 261529 and a grant from The Isaac Newton Trust, Trinity College,
457 Cambridge. M.Paul acknowledges funding by the German Science Foundation (grant no. PA 2547/1-
458 1).
459

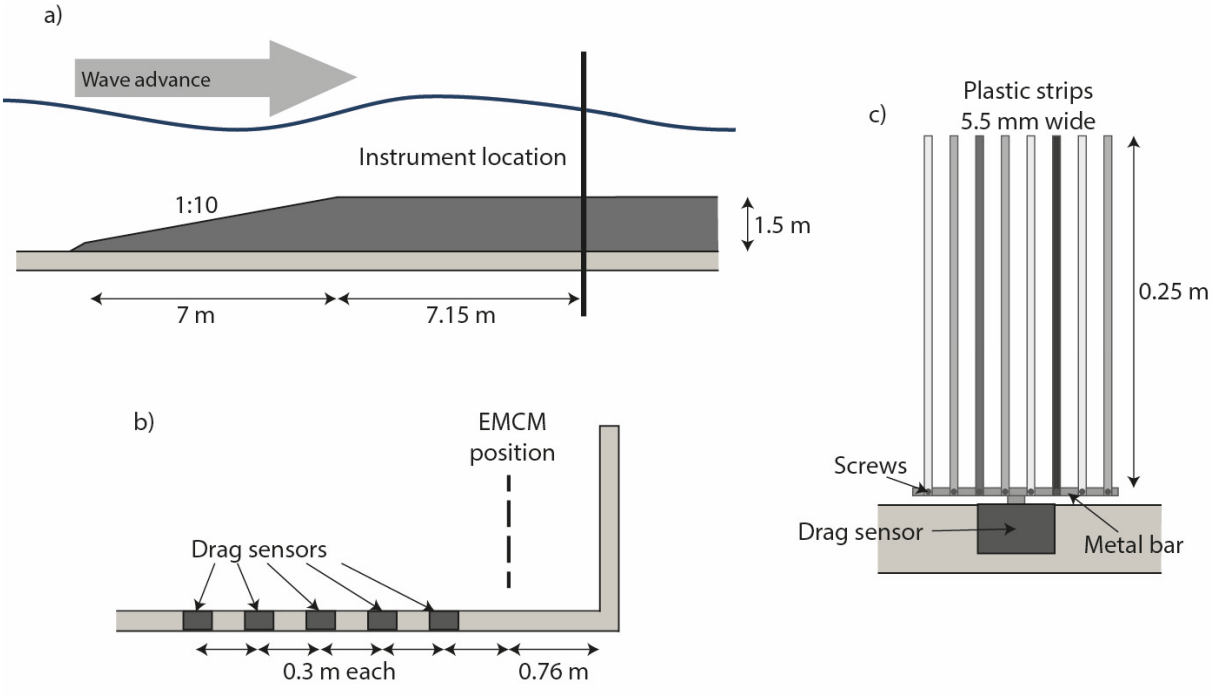

460

461 **Figure 1: Schematic of instrument setup indicating a) the instrument location in a flume side view, b) a downstream view**
462 **of the instrument location, and c) the mounting of strip arrangements on the drag sensors. At the black position a strip**
463 **was attached for all arrangements. In addition, the dark shaded position was used for the 2 x 4 mm arrangement, for the**
464 **4 x 2 mm arrangement the medium shaded positions were used and the 8 x 2 mm and 8 x 1 mm arrangements used all**
465 **positions.**

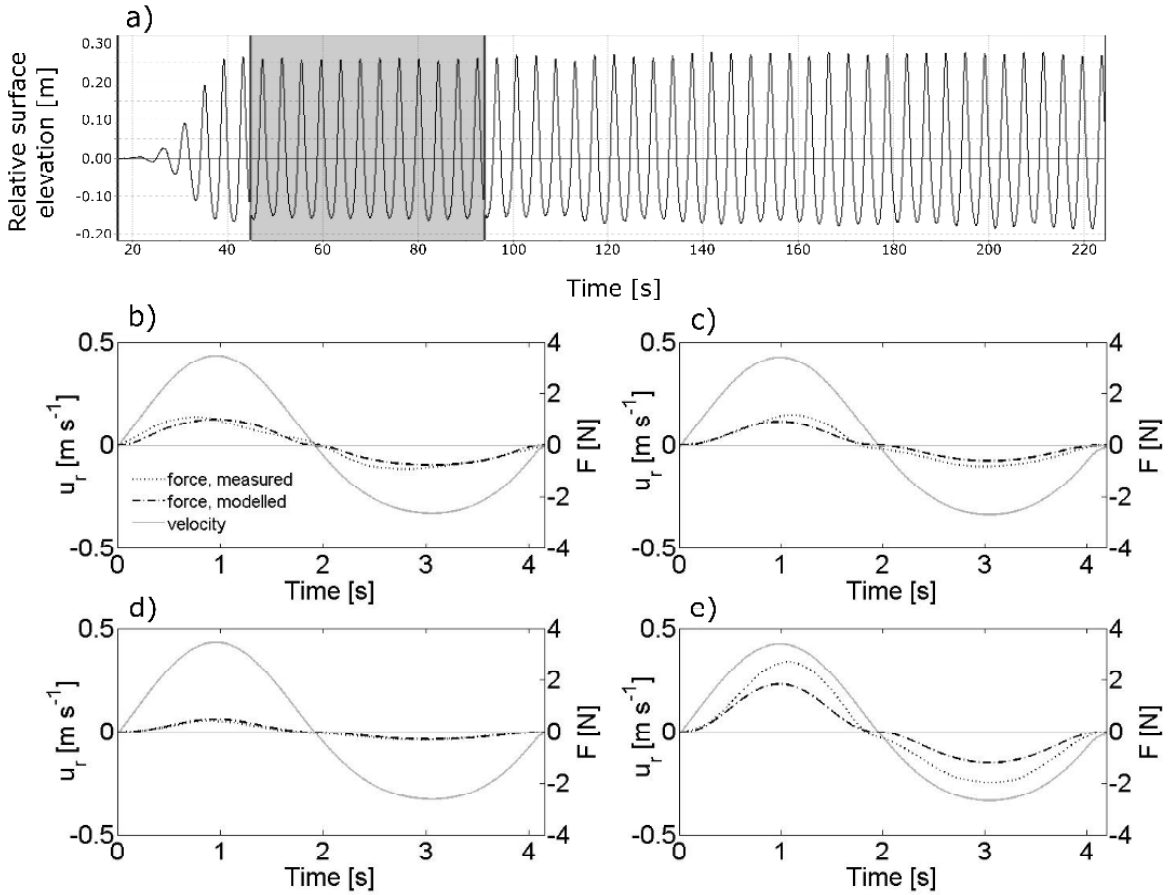

Figure 2: Time series of relative surface elevation under regular waves (*H* = 0.4 m, *T* = 4.1 s) in 2 m water depth with the grey shaded area indicating the first 11 fully developed waves used for analysis (a) and time series of averaged horizontal velocity and drag forces under the same conditions for b) the 8 x 1 mm arrangement (R^2 = 0.97, RMSE = 0.11, absolute maximum residual = 0.30), c) the 4 x 2 mm arrangement (R^2 = 0.95, RMSE = 0.11, absolute maximum residual = 0.49), d) the 2 x 4 mm arrangement (R^2 = 0.92, RMSE = 0.07, absolute maximum residual = 0.21), and e) 8 x 2 mm arrangement (R^2 = 0.96, RMSE = 0.21, absolute maximum residual = 0.68). R^2 gives the linear regression fit between measured and modelled force time series and RMSE is the root-mean-square error of this fit. These are illustrative examples; all other tests showed the same quality of model fit.

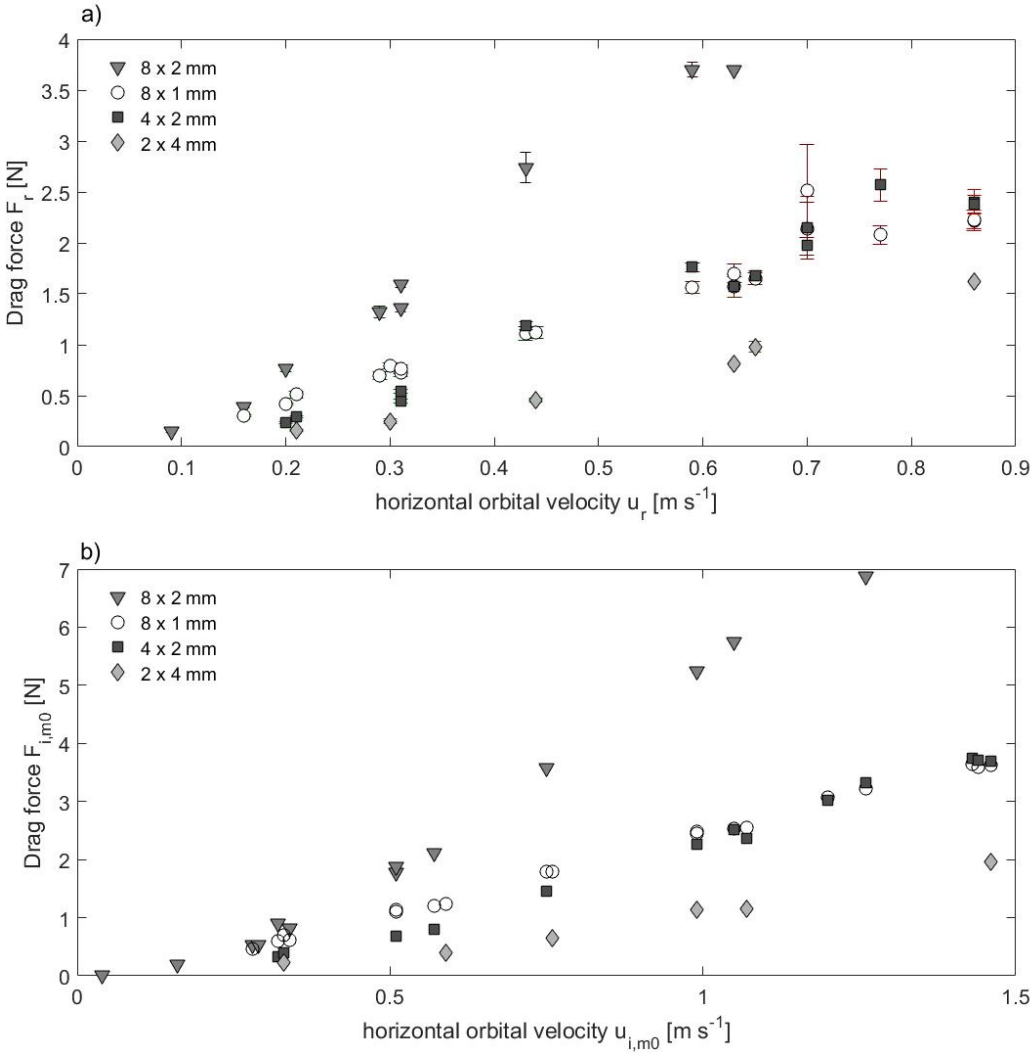

478

479

480 **Figure 3: Drag forces for the different mimic arrangements in relationship to a) maximum horizontal orbital velocity $u_{r,max}$**

481 **for regular waves, b) horizontal orbital velocity $u_{i,m0}$ for irregular waves. For regular waves values are given with ± one**

482 **standard deviation. Values for mimic arrangements are corrected for the influence of the horizontal metal bar.**

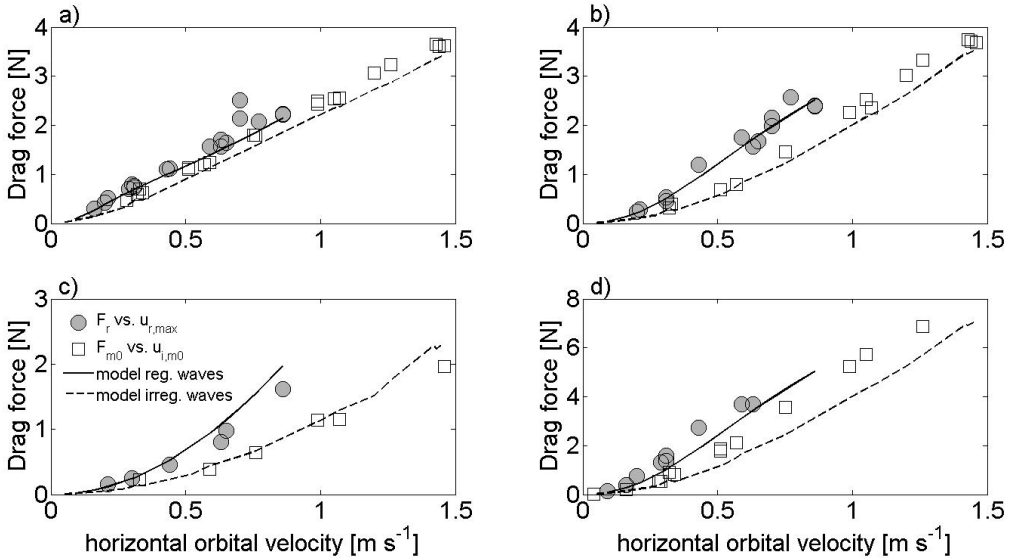

483

Figure 4: Measured drag forces and the fitted Luhar and Nepf (2011) model for the different mimic arrangements a) 8 x 1 mm, b) 4 x 2 mm, c) 2 x 4 mm, and d) 8 x 2 mm in relationship to horizontal orbital velocity 15 cm above the bed for regular and irregular waves. Standard deviation for the regular wave data is omitted for clarity.

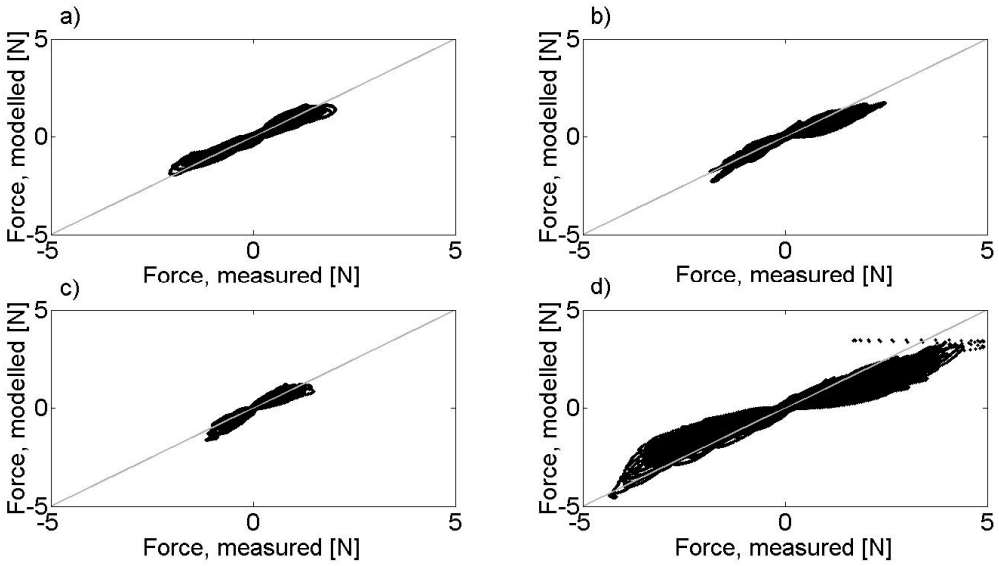

Figure 5: Scatter plot of the modelled forces vs. measured forces for irregular waves (H_{m0} = 0.4 m, T_p = 4.13 s) in 2 m water depth. The grey line depicts $F_{modelled} = a*F_{measured}$ with a = 1. For each dataset, a was computed using linear regression for a) the 8 x 1 mm arrangement (a = 0.85, R^2 = 0.94, RMSE = 0.09, absolute maximum residual = 0.54), b) the 4 x 2 mm arrangement (a = 0.80, R^2 = 0.91, RMSE = 0.09, absolute maximum residual = 0.88), c) the 2 x 4 mm arrangement (a = 0.96, R^2 = 0.86, RMSE = 0.06, absolute maximum residual = 0.65), and d) the 8 x 2 mm arrangement (a = 0.66, R^2 = 0.92, RMSE = 0.18, absolute maximum residual = 2.35). R^2 gives the linear regression fit between measured and modelled force time series and RMSE is the root-mean-square error of this fit.

Table 1: Parameters of the used mimic arrangements and goodness-of-fit parameters for the Luhar and Nepf (2011) model. Flexural rigidity is given ± standard deviation. The fit parameters refer to the relationship $F_{modelled} = a*F_{measured}$ for F_r and F_{m0} respectively across the whole velocity range tested, for the data shown in Figure 4.

Arrangement	Number of strips	Strip thickness (mm)	Still frontal area (cm^2)	Material volume (cm^3)	Flexural rigidity (Nm^2)	Fit parameter $a_{regular}$/ R^2	Fit parameter $a_{irregular}$/ R^2
8 x 1 mm	8	1	110	11	$1.36*10^{-3} \pm 3.73*10^{-5}$ (n = 9)	0.88/ 0.94	0.91/ 0.99
4 x 2 mm	4	2	55	11	$8.97*10^{-3} \pm 6.73*10^{-5}$ (n = 10)	0.97/ 0.96	0.91/ 0.99
2 x 4 mm	2	4	27.5	11	$6.57*10^{-2} \pm 3.21*10^{-3}$ (n = 10)	1.21/ 0.99	1.12/ 0.98
8 x 2 mm	8	2	110	22	$8.97*10^{-3} \pm 6.73*10^{-5}$ (n = 10)	0.82/ 0.96	0.77/ 0.99

500 **References**

501 Aberle, J., Järvelä, J., 2013. Flow resistance of emergent rigid and flexible floodplain vegetation.
502 Journal of Hydraulic Research 51 (1), 33–45. doi:10.1080/00221686.2012.754795.

503 Augustin, L.N., Irish, J.L., Lynett, P., 2009. Laboratory and numerical studies of wave damping by
504 emergent and near-emergent wetland vegetation. Coastal Engineering 56, 332–340.
505 doi:10.1016/j.coastaleng.2008.09.004.

506 Barbier, E.B., Koch, E.W., Silliman, B.R., Hacker, S.D., Wolanski, E., Primavera, J.H., Granek, E.F.,
507 Polansky, S., Aswani, S., Cramer, L.A., Stoms, D.M., Kennedy, C.J., Bael, D., Kappel, C.V., Perillo,
508 G.M.E., Reed, D.J., 2008. Coastal Ecosystem - Based Management with Nonlinear Ecologial
509 Functions and Values. Science 319. doi:10.1126/science.1150349.

510 Bell, E.C., 1999. Applying flow tank measurements to the surf zone: predicting dislodgement of the
511 Gigartinaceae. Phycological Research 47, 159–166.

512 Boller, M.L., Carrington, E., 2006. The hydrodynamic effects of shape and size change during
513 reconfiguration of a flexible macroalga. Journal of Experimental Biology 209 (10), 1894–1903.
514 doi:10.1242/jeb.02225.

515 Bouma, T.J., de Vries, M.B., Herman, P.M.J., 2010. Comparing ecosystem engineering efficiency of 2
516 plant species with contrasting growth strategies. Ecology 91 (9), 2696–2704. doi:10.1890/09-
517 0690.1.

518 Bouma, T.J., de Vries, M.B., Low, E., Peralta, G., Tánczos, I.C., van de Koppel, J., Herman, P.M.J., 2005.
519 Trade-offs related to ecosystem engineering: A case study on stiffness of emerging macrophytes.
520 Ecology 86 (8), 2187–2199. doi:10.1890/04-1588.

521 Bouma, T.J., Friedrichs, M., van Wesenbeeck, B.K., Temmerman, S., Graf, G., Herman, P.M.J., 2009.
522 Density-dependent linkage of scale-dependent feedbacks: a flume study on the intertidal
523 macrophyte Spartina anglica. Oikos 118 (2), 260–268. doi:10.1111/j.1600-0706.2008.16892.x.

524 Bouma, T.J., van Belzen, J., Balke, T., Zhu, Z., Airoldi, L., Blight, A.J., Davies, A.J., Galván, C., Hawkins,
525 S.J., Hoggart, S.P., Lara, J.L., Losada, I.J., Maza, M., Ondiviela, B., Skov, M.W., Strain, E.M.,

526 Thompson, R.C., Yang, S., Zanuttigh, B., Zhang, L., Herman, P.M.J., 2014. Identifying knowledge
527 gaps hampering application of intertidal habitats in coastal protection: Opportunities & steps to
528 take. Coastal Engineering 87, 147–157. doi:10.1016/j.coastaleng.2013.11.014.
529 Bradley, K., Houser, C., 2009. Relative velocity of seagrass blades: Implications for wave attenuation
530 in low-energy environments. J. Geophys. Res. 114 (F01004), 1–13. doi:10.1029/2007JF000951.
531 Callaghan, F.M., Cooper, G.G., Nikora, V.I., Lamouroux, N., Statzner, B., Sagnes, P., Radford, J., Malet,
532 E., Biggs, B.J., 2007. A submersible device for measuring drag forces on aquatic plants and other
533 organisms. New Zealand Journal of Marine and Freshwater Research 41 (1), 119–127.
534 doi:10.1080/00288330709509900.
535 Carrington, E., 1990. Drag and Dislodgment of an Intertidal Macroalga - Consequences of
536 Morphological Variation in Mastocarpus-Papillatus Kutzing. Journal of Experimental Marine
537 Biology and Ecology 139 (3), 185–200. doi:10.1016/0022-0981(90)90146-4.
538 Chen, L., Stone, M.C., Acharya, K., Steinhaus, K.A., 2011. Mechanical analysis for emergent vegetation
539 in flowing fluids. Journal of Hydraulic Research 49 (6), 766–774.
540 doi:10.1080/00221686.2011.621359.
541 Dalrymple, R.A., Kirby, J.T., Hwang, P.A., 1984. Wave diffraction due to areas of energy dissipation. J.
542 Wtrwy., Port, Coast., and Oc. Engrg. 110 (1), 67–79. doi:10.1061/(ASCE)0733-
543 950X(1984)110:1(67).
544 Denny, M.W., 1988. Biology and the mechanics of the wave swept environment. Princeton University
545 Press, Princeton, New Jersey.
546 Denny, M.W., Gaylord, B., 2002. The mechanics of wave-swept algae. Journal of Experimental Biology
547 205 (10), 1355–1362.
548 Denny, M.W., Gaylord, B., Helmuth, B., Daniel, T., 1998. The menace of momentum: Dynamic forces
549 on flexible organisms. Limnol. Oceangr 43 (5), 955–968. doi:10.4319/lo.1998.43.5.0955.

550 Eckman, J., Werner, F.E., Gross, T.F., 1994. Modelling some effects of behavior on larval settlement in
551 a turbulent boundary layer. Deep-Sea Research 41 (1), 185–208. doi:10.1016/0967-
552 0645(94)90067-1.
553 Gaylord, B., Denny, M.W., 1997. Flow and flexibility: I. Effects of size, shape and stiffness in
554 determining wave forces on the stipitate kelps Eisenia arborea and Pterygophora californica.
555 Journal of Experimental Biology 200, 3141–3164.
556 Gaylord, B., Denny, M.W., Koehl, M.A.R., 2003. Modulation of wave forces on kelp canopies by
557 alongshore currents. Limnol. Oceangr 48 (2), 860–871. doi:10.4319/lo.2003.48.2.0860.
558 Henry, P.-Y.T., 2014. Bending properties of a macroalga: Adaptation of Peirce's cantilever test for in
559 situ measurements of Laminaria digitata (Laminariaceae). American Journal of Botany 101 (6),
560 1050–1055. doi:10.3732/ajb.1400163.
561 Henry, P.-Y.T., Myrhaug, D., 2013. Wave-induced drag force on vegetation under shoaling random
562 waves. Coastal Engineering 78, 13–20. doi:10.1016/j.coastaleng.2013.03.004.
563 Henry, P.-Y.T., Myrhaug, D., Aberle, J., 2015. Drag forces on aquatic plants in nonlinear random
564 waves plus current. Estuarine, Coastal and Shelf Science 165, 10–24.
565 doi:10.1016/j.ecss.2015.08.021.
566 Houser, C., Trimble, S., Morales, B., 2015. Influence of Blade Flexibility on the Drag Coefficient of
567 Aquatic Vegetation. Estuaries and Coasts 38 (2), 569–577. doi:10.1007/s12237-014-9840-3.
568 Lightbody, A.F., Nepf, H.M., 2006. Prediction of velocity profiles and longitudinal dispersion in
569 emergent salt marsh vegetation. Limnol. Oceangr 51 (1), 218–228.
570 doi:10.4319/lo.2006.51.1.0218.
571 Luhar, M., Nepf, H.M., 2011. Flow-induced reconfiguration of buoyant and flexible aquatic
572 vegetation. Limnol. Oceangr 56 (6), 2003–2017. doi:10.4319/lo.2011.56.6.2003.
573 Maza, M., Lara, J.L., Losada, I.J., 2013. A coupled model of submerged vegetation under oscillatory
574 flow using Navier–Stokes equations. Coastal Engineering 80, 16–34.
575 doi:10.1016/j.coastaleng.2013.04.009.

576 Méndez, F.J., Losada, I.J., 2004. An empirical model to estimate the propagation of random breaking
577 and nonbreaking waves over vegetation fields. Coastal Engineering 51 (2), 103–118.
578 doi:10.1016/j.coasaleng.2003.11.003.
579 Möller, I., Kudella, M., Rupprecht, F., Spencer, T., Paul, M., van Wesenbeeck, B.K., Wolters, G.,
580 Jensen, K., Bouma, T.J., Miranda-Lange, M., Schimmels, S., 2014. Wave attenuation over coastal
581 salt marshes under storm surge conditions. Nature Geosci 7 (10), 727–731.
582 doi:10.1038/ngeo2251.
583 Möller, I., Spencer, T., French, J.R., Leggett, D.J., Dixon, M., 1999. Wave transformation over salt
584 marshes: a field and numerical modelling study from North Norfolk, England. Estuarine, Coastal
585 and Shelf Science 49, 411–426. doi:10.1006/ecss.1999.0509.
586 Mullarney, J.C., Henderson, S.M., 2010. Wave-forced motion of submerged single-stem vegetation.
587 Journal of Geophysical Research - Oceans 115 (C12061), 1–14. doi:10.1029/2010JC006448.
588 O'Hare, M.T., Hutchinson, K.A., Clarke, R.T., 2007. The drag and reconfiguration experienced by five
589 macrophytes from a lowland river. Aquatic Botany 86 (3), 253–259.
590 doi:10.1016/j.aquabot.2006.11.004.
591 Paul, M., Amos, C.L., 2011. Spatial and seasonal variation in wave attenuation over Zostera noltii. J.
592 Geophys. Res. 116, C08019. doi:10.1029/2010JC006797.
593 Paul, M., Bouma, T.J., Amos, C.L., 2012. Wave attenuation by submerged vegetation: combining the
594 effect of organism traits and tidal current. Mar. Ecol. Prog. Ser. 444, 31–41.
595 doi:10.3354/meps09489.
596 Penning, W.E., Raghuraj, R., Mynett, A., 2009. The effect of macrophyte morphology and patch
597 density on wave attenuation, in: Proceedings of 7th ISE and 8th HIC, Chile.
598 Peralta, G., van Duren, L.A., Morris, E.P., Bouma, T.J., 2008. Consequences of shoot density and
599 stiffness for ecosystem engineering by benthic macrophytes in flow dominated areas: a
600 hydrodynamic flume study. Mar. Ecol. Prog. Ser. 368, 103–115.

601 Ravenell, J., Seixas, A., Rosenthal, D.M., Williams, O., Ogedegbe, C., Sevick, M.A., Newsome, V., Jean-
602 Louis, G., 2016. Effect of birthplace on cardiometabolic risk among blacks in the Metabolic
603 Syndrome Outcome Study (MetSO). Diabetology & metabolic syndrome 8, 14.
604 doi:10.1061/(ASCE)0733-950X(1993)119:1(30).
605 Rupprecht, F., Möller, I., Evans, B., Spencer, T., Jensen, K., 2015. Biophysical properties of salt marsh
606 canopies — Quantifying plant stem flexibility and above ground biomass. Coastal Engineering
607 100, 48–57. doi:10.1016/j.coastaleng.2015.03.009.
608 Sand-Jensen, K., 2003. Drag and reconfiguration of freshwater macrophytes. Freshwater Biol 48 (2),
609 271–283. doi:10.1046/j.1365-2427.2003.00998.x.
610 Schoneboom, T., Aberle, J., Dittrich, A., 2010. Hydraulic resistance of vegetated flows: Contribution of
611 bed shear stress and vegetative drag to total hydraulic resistance, in: Proceedings of the
612 International Conference on Fluvial Hydraulics River Flow 2010. River Flow 2010, Braunschweig,
613 Germany, pp. 269–276.
614 Schoneboom, T., Aberle, J., Dittrich, A., 2011. Spatial Variability, Mean Drag Forces, and Drag
615 Coefficients in an Array of Rigid Cylinders, in: Rowinski, P. (Ed.), Experimental Methods in
616 Hydraulic Research, vol. 1. Springer Berlin Heidelberg, Berlin, Heidelberg, pp. 255–265.
617 Siniscalchi, F., Nikora, V.I., 2012. Flow-plant interactions in open-channel flows: A comparative
618 analysis of five freshwater plant species. Water Resour. Res. 48 (5). doi:10.1029/2011WR011557.
619 Siniscalchi, F., Nikora, V.I., Aberle, J., 2012. Plant patch hydrodynamics in streams: Mean flow,
620 turbulence, and drag forces. Water Resour. Res. 48 (1). doi:10.1029/2011WR011050.
621 Sparboom, U., Hildebrandt, A., Oumeraci, H., 2006. Group interaction effects of slender cylinders
622 under wave attack, in: Proceedings 30th International Conference on Coastal Engineering (ICCE),
623 San Diego, USA, pp. 4430–4442.
624 Statzner, B., Lamouroux, N., Nikora, V.I., Sagnes, P., 2006. The debate about drag and reconfiguration
625 of freshwater macrophytes: comparing results obtained by three recently discussed approaches.
626 Freshwater Biol 51 (11), 2173–2183. doi:10.1111/j.1365-2427.2006.01636.x.

627 Stratigaki, V., Manca, E., Prinos, P., Losada, I.J., Lara, J.L., Sclavo, M., Amos, C.L., Cáceres, I., Sánchez-
628 Arcilla, A., 2011. Large-scale experiments on wave propagation over Posidonia oceanica. Journal
629 of Hydraulic Research 49 (sup1), 31–43. doi:10.1080/00221686.2011.583388.
630 Temmerman, S., Meire, P., Bouma, T.J., Herman, P.M.J., Ysebaert, T., De Vriend, Huib J., 2013.
631 Ecosystem-based coastal defence in the face of global change. Nature 504 (7478), 79–83.
632 doi:10.1038/nature12859.
633 Vogel, S., 1994. Life in moving fluids: the physical biology of flow, 2nd ed. Princeton University Press,
634 Princeton, N.J.
635 Yang, S.L., Shi, B.W., Bouma, T.J., Ysebaert, T., Luo, X.X., 2012. Wave Attenuation at a Salt Marsh
636 Margin: A Case Study of an Exposed Coast on the Yangtze Estuary. Estuaries and Coasts 35 (1),
637 169–182. doi:10.1007/s12237-011-9424-4.
638
639